

Direct extraction of the Eliashberg function for electron-phonon coupling: A case study of Be(10 $\bar{1}0$)

Junren Shi,¹ S.-J. Tang,² Biao Wu,^{1,3} P.T. Sprunger,⁴ W.L. Yang,^{5,6} V. Brouet,^{5,6}

X.J. Zhou,⁵ Z. Hussain,⁶ Z.-X. Shen,⁵ Zhenyu Zhang,^{1,2} E.W. Plummer^{1,2}

¹Condensed Mater Sciences Division, Oak Ridge National Laboratory, Oak Ridge, TN 37831

²Department of Physics and Astronomy, University of Tennessee, Knoxville, TN 37996

³Department of Physics, University of Texas, Austin, TX 78712

⁴Department of Physics and Astronomy, Louisiana State University, Baton Rouge, LA 70803

⁵Department of Physics, Applied Physics and Stanford Synchrotron Radiation Laboratory, Stanford University, Stanford, CA 94305

⁶Advanced Light Source, Lawrence Berkeley National Laboratory, Berkeley, CA 94720

We propose a systematic procedure to directly extract the Eliashberg function for electron-phonon coupling from high-resolution angle-resolved photoemission data. The procedure is successfully applied to the Be(10 $\bar{1}0$) surface, providing new insights to electron-phonon coupling at this surface. The method is shown to be robust against imperfections in experimental data and suitable for wider applications.

PACS numbers: 71.38.-k, 73.20.-r

Electron-phonon coupling (EPC) is the basis for many interesting phenomena in condensed matter physics such as conventional superconductivity. Its possible role in the high- T_c superconductivity is also being actively discussed [1, 2]. Experimentally, recent advances in high-resolution (both energy and momentum) angle-resolved photoemission spectroscopy (ARPES) have stimulated many studies on EPC in various systems [1–11]. These ARPES measurements usually yield the mass enhancement factor λ [12], which characterizes the strength of the EPC, along with some rough ideas about its spectral structure such as the dominant phonon mode. It is then desirable to take advantage of these high-resolution data and obtain full characteristics of EPC.

Theoretically, the full characteristics of EPC are described by the Eliashberg function $\alpha^2 F(\omega; \epsilon, \mathbf{k})$ [12]. The function provides a measure of the strength of EPC, as well as its spectral structure. All quantities characterizing EPC-related effects can be deduced from the function. For instance, the mass enhancement factor λ is related to the Eliashberg function at the Fermi surface by [12],

$$\lambda = 2 \int_0^{\infty} \frac{d\omega}{\omega} \alpha^2 F(\omega; \epsilon_F, \hat{\mathbf{k}}). \quad (1)$$

In this Letter, we present a systematic procedure to directly extract the Eliashberg function at the Fermi surface from the high-resolution ARPES data. The Maximum Entropy Method (MEM) [13] is employed to make a statistical estimate of the Eliashberg function in a numerically stable way. With Eq.1, it also gives a reliable evaluation of the mass enhancement factor λ , without making assumption on phonon model or requiring low measurement temperature [4–11].

This procedure is illustrated using new high-resolution ARPES data at the Be(10 $\bar{1}0$) surface. This system is ideal for testing the new procedure because Be is a light element which is rigidly bound in the crystal and the top of its phonon bands is at ~ 80 meV, removing the need for super-high-energy resolution. Also, measurements [14] and theoretical calculations [16] of the phonon dispersion at this surface have been published, providing references for comparison.

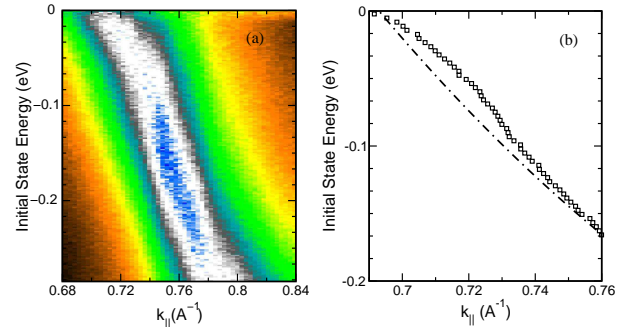


Figure 1: (a) Photoemission image of the S1 surface state of Be(10 $\bar{1}0$) along $\bar{A}\bar{\Gamma}$ (origin is at $\bar{\Gamma}$) near the Fermi energy. (b) Quasi-particle dispersion determined from the momentum distribution curves. The dashed-dotted line indicates $\epsilon_0(\mathbf{k})$ (see text).

The photoemission experiments were performed at the Advanced Light Source (ALS) on Beamline 10.0.1 using a display high-resolution Scienta 2002 energy analyzer at 40 eV photon energy with total energy resolution 10 meV and angular resolution $\pm 0.15^\circ$ in 6×10^{-11} Torr vacuum and at $T = 30$ K. The cleaning procedure for the Be(10 $\bar{1}0$) sample was described earlier [4]. Fig. 1(a) shows the photoemission image of the S1 surface state that is present at the surface Brillouin zone (SBZ) boundary of Be(10 $\bar{1}0$). The mass enhancement factor λ for S_1 was previously measured using temperature dependent line-shape at the band bottom \bar{A} that is 0.37 eV below the Fermi surface, yielding a value $\lambda_{\bar{A}} = 0.65$ [9].

Figure 1(b) shows the band dispersion of the S1 surface state near the Fermi surface determined from momentum distribution curves [7]. The distortion of the surface state dispersion can be clearly seen within the energy scale of the Be phonon bandwidth (80 meV). In general, the quasi-particle dispersion can be written as,

$$\epsilon(\mathbf{k}) = \epsilon_0(\mathbf{k}) + \text{Re}\Sigma(\mathbf{k}, \epsilon), \quad (2)$$

where $\Sigma(\mathbf{k}, \epsilon)$ is the electron self-energy and $\epsilon_0(\mathbf{k})$ is the dispersion for the quasi-particle in a frozen lattice (i.e., without EPC). Following the extrapolation procedure described in

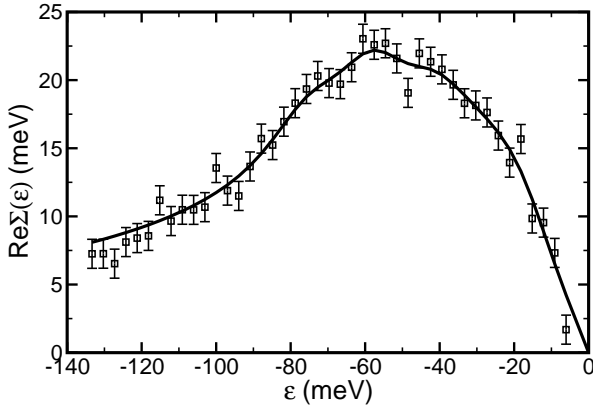


Figure 2: The real part of the self energy determined from the quasi-particle dispersion (see Fig. 1) for the S1 surface state. Solid line shows the MEM fitting (classic method) for the data. The error bars (σ_i) are assumed to be constant for all data points and determined statistically from the noise of the data, which yield a value 1.1 meV.

Ref. 7, we determine $\epsilon_0(\mathbf{k}) \approx -v_F^0(k - k_F) + a(k - k_F)^2$ with $v_F^0 = 2.90 \text{ eV} \cdot \text{\AA}$, $a = 6.74 \text{ eV} \cdot \text{\AA}^2$ and $k_F = 0.693 \text{ \AA}^{-1}$, as shown in Fig. 1(b). The real part of the electron self-energy for the S1 state is determined by Eq. 2, and it is shown in Fig. 2.

In principle, the Eliashberg function can be directly extracted from the real part of the electron self-energy, which is related to the Eliashberg function by [12]:

$$\text{Re}\Sigma(\hat{\mathbf{k}}, \epsilon; T) = \int_0^\infty d\omega \alpha^2 F(\omega; \epsilon, \hat{\mathbf{k}}) G\left(\frac{\epsilon}{kT}, \frac{\omega}{kT}\right), \quad (3)$$

where

$$G(y, y') = \int_{-\infty}^\infty dx \frac{2y'}{x^2 - y'^2} f(x + y), \quad (4)$$

with $f(x)$ being the Fermi distribution function. The full Eliashberg function $\alpha^2 F(\omega; \epsilon, \hat{\mathbf{k}})$ is a function of the phonon frequency ω , electron initial state energy $\epsilon = \epsilon(\mathbf{k})$, and momentum direction $\hat{\mathbf{k}}$ [12, 15]. In our case, dependence on the electron initial state energy ϵ can be ignored because it only varies around the Fermi surface within a small energy scale that is the order of surface phonon bandwidth, and $d\alpha^2 F(\omega; \epsilon, \hat{\mathbf{k}})/d\omega \gg d\alpha^2 F(\omega; \epsilon, \hat{\mathbf{k}})/d\epsilon$. As a result, the full Eliashberg function in Eq. 3 can be replaced by the Eliashberg function at the Fermi surface $\alpha^2 F(\omega; \epsilon_F, \hat{\mathbf{k}})$, and Eqs. 3-4 define the integral inversion problem for extracting the Eliashberg function at the Fermi surface from the real part of the electron self-energy. For brevity, the Eliashberg function $\alpha^2 F(\omega) \equiv \alpha^2 F(\omega; \epsilon_F, \hat{\mathbf{k}})$ refers to the Eliashberg function at the Fermi surface, and the explicit dependence on the momentum direction $\hat{\mathbf{k}}$ is also dropped.

The most straightforward way to do the integral inversion is the least-squares approach that minimizes the functional:

$$\chi^2 = \sum_{i=1}^{N_D} \frac{[D_i - \text{Re}\Sigma(\epsilon_i)]^2}{\sigma_i^2}, \quad (5)$$

against the Eliashberg function $\alpha^2 F(\omega)$, where D_i is the data of the real part of electron self-energy at electron energy ϵ_i ; $\text{Re}\Sigma(\epsilon_i)$ is defined by Eq. 3 and is a functional of the Eliashberg function $\alpha^2 F(\omega)$ to be fitted; σ_i is the error bar for the experimental data D_i ; and N_D is the total number of data points. Unfortunately, because of the data noise inevitably presented, such a straightforward approach fails to provide any useful information because the inversion problem defined by Eqs. 3-4 is ill-posed mathematically and the direct inversion tends to exponentially amplify the high-frequency data noise, resulting in great fluctuations and negative values in the extracted Eliashberg function [17].

The failure of the least-squares method originates from the fact that we do not incorporate physical constraints (*priori* knowledge) in the fitting process. One constraint is that the Eliashberg function must be positive. The standard way to incorporate the constraints in the fitting process is the Maximum Entropy Method. The statistical argument suggests that to determine the spectrum density like the Eliashberg function, the following functional should be minimized [13],

$$L = \frac{\chi^2}{2} - aS \quad (6)$$

where χ^2 is defined in Eq. 5, and S is the generalized Shannon-Jaynes entropy,

$$S = \int_0^\infty d\omega \left[\alpha^2 F(\omega) - m(\omega) - \alpha^2 F(\omega) \ln \frac{\alpha^2 F(\omega)}{m(\omega)} \right]. \quad (7)$$

The constraint function $m(\omega)$ represents our best knowledge for the function to be fitted before knowing any data (*priori* knowledge). The entropy is maximized when $\alpha^2 F(\omega) = m(\omega)$.

The multiplier a controls the balance between minimizing χ^2 and maximizing the entropy S . When a is small, the experimental data are emphasized, and the fitting follows the data as closely as possible; in the opposite limit, the entropy is emphasized, and the extracted Eliashberg function cannot move far away from $m(\omega)$. In this study, we employ the classic method [13] in choosing the optimized value of a . The Newton algorithm is applied to optimize Eq. 6 [13]. The iterated trapezoid rule is used to approximate the integral over ω in Eq. 3 and 7. Detailed and comprehensive reviews on the MEM algorithms can be found in Ref. 13.

The constraint function $m(\omega)$ should be chosen in such a way that it reflects our best knowledge for the Eliashberg function of the specific system. For Be(10 $\bar{1}$ 0), as well as for many other systems, no detailed knowledge of the Eliashberg function is available except some general physical constraint: (a) it is positive; (b) it vanishes at the limit $\omega \rightarrow 0$; and (c) it vanishes above the maximal phonon frequency. To reflect these, we use the following generic form:

$$m(\omega) = \begin{cases} m_0 (\omega/\omega_R)^2, & \omega \leq \omega_R \\ m_0, & \omega_R < \omega \leq \omega_m \\ 0, & \omega > \omega_m \end{cases}, \quad (8)$$

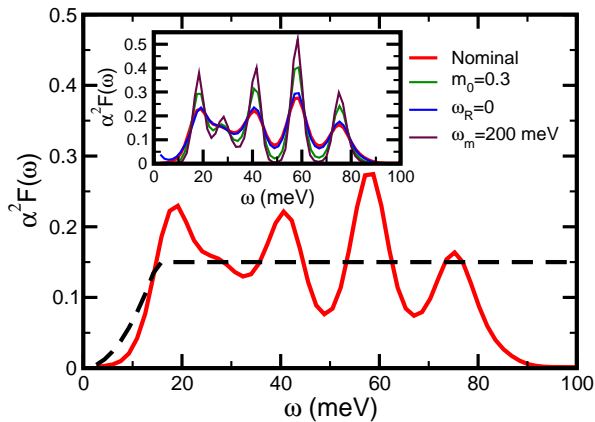


Figure 3: (a) Extracted Eliashberg function for S1 surface state of Be(10 $\bar{1}$ 0). The dashed line shows $m(\omega)$ with parameters $\omega_R = 15$ meV, $\omega_m = 100$ meV, and $m_0 = 0.15$. Inset: effects of the different fitting parameters. Each line shows the result by changing one of the parameters used in the main figure, as indicated by the legends.

The dependence on the parameters ω_R , ω_m , and m_0 will be discussed later.

Figure 3 shows the estimate of the Eliashberg function of the Be(10 $\bar{1}$ 0) S1 surface state. It successfully resolves a number of peaks roughly at 40, 60, and 75 meV. A low energy mode at $\omega < 30$ meV is also evident. When compared with the first-principles calculations of the phonon dispersion [16], the positions of the peaks have good correspondence to the frequencies of those surface phonon modes. The extracted Eliashberg function automatically cuts off at roughly 80 meV, which is also consistent with the calculation result [16]. Note that there is no freely adjustable parameter in our fitting scheme except three parameters, m_0 , ω_R , and ω_m , which, as will be shown below, do not change the qualitative result. The mass enhancement factor λ defined at the Fermi surface is calculated by Eq. 1, yielding a value 0.65 ± 0.06 , which is greatly enhanced from the bulk value 0.24.

We have carried out systematic studies to assess the effects of the parameters m_0 , ω_R , and ω_m . These parameters may influence the decision of the classic algorithm in choosing the optimized value of a , thus affecting the result. In calculating the nominal estimate shown in Fig. 3, we choose these parameters in such a way that the resulting $m(\omega)$ matches the overall shape of the extracted Eliashberg function closely. The inset in Fig. 3 shows a few extreme cases for the effects of the different parameters: Changing ω_R will affect the behavior near the zero frequency, and a non-zero ω_R is important to guarantee the correct low-frequency behavior. Changing m_0 and ω_m has little qualitative effect besides affecting the ‘‘contrast’’ of the results. Note that all the physical features of the extracted Eliashberg function (e.g., the number and the positions of the peaks, the highest phonon frequency) are intact. Furthermore, the estimated values of the mass enhancement factor λ are not sensitive to the parameters used. For the cases shown in the inset of Fig. 3, the calculated λ are 0.71 ± 0.20

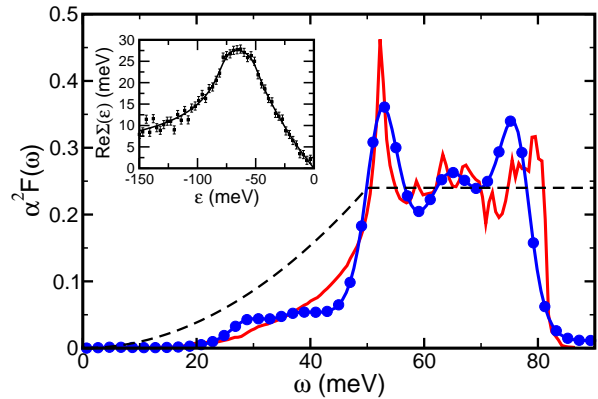


Figure 4: (Color online) A test to the data extraction procedure. Solid line shows the pre-defined Eliashberg function. The filled circle-line shows the extracted Eliashberg function. Dashed line shows $m(\omega)$ with parameters $\omega_R = 50$ meV, $\omega_m = 100$ meV, and $m_0 = 0.24$. Inset shows the data presented to the program and the comparison with the MEM fitting. Gaussian noise (non-correlated between different data points) with a mean deviation $\sigma = 1$ meV has been added to the self-energy data. $T = 30$ K.

for $\omega_R = 0$, 0.63 ± 0.06 for $m_0 = 0.3$, and 0.62 ± 0.05 for $\omega_m = 200$ meV, respectively. We conclude that the parameters in our fitting do not affect the physical conclusions.

To test the reliability of the procedure and see how well it reproduces the true result, we generate a set of data of the real part of self-energy from a pre-defined Eliashberg function. Gaussian noise is added to simulate the realistic experimental situation. The comparison between the extracted spectrum and the pre-defined Eliashberg function provides a test. Figure 4 shows a typical result. It can be seen that the MEM successfully extracted the overall qualitative features of the predefined Eliashberg function although the data are rather noisy. The mass enhancement factor calculated from Eq. 1 is 0.35 ± 0.05 , which is very close to the exact value 0.35. We observe that such a close match between the extracted value of λ and the exact value is rather common in the test cases we have performed.

The major advantage of the MEM over the traditional technique [17] is its robustness against data imperfections. We observe that: (a) the error in determining $\epsilon_0(\mathbf{k})$ (see Eq. 2), i.e., the value of ν_F^0 , has little effect on the extracted Eliashberg function. An inappropriate value of ν_F^0 would induce incorrect asymptotic behavior in the high binding energy regime of $\text{Re}\Sigma(\epsilon)$, but this can be easily detected and corrected in the fitting procedure; (b) the algorithm puts appropriate weight on those abnormal data points (for instance, like the one near 50 meV in Fig. 2), preventing them from dramatically distorting the extracted Eliashberg function; (c) we have assumed constant error bars σ_i for all the data points. A more realistic distribution with larger error bars in the high binding energy regime has no significant effect on the extracted Eliashberg function.

As another advantage of the MEM, the constraint function $m(\omega)$ provides a systematic mechanism to progressively im-

prove the fitting and incorporate existing knowledge. For instance, if the phonon density of states $F(\omega)$ is known from other reliable sources, one can assume $m(\omega) = \alpha_0^2 \times F(\omega)$ with α_0^2 being determined by optimizing its posterior probability [13]. Such a scheme should allow a seamless integration of the existing knowledge about the fine spectral structure and the newly extracted knowledge about the coupling strengths.

Besides the advantages of the MEM, the new technique is promising also because: (a) The new procedure based on the ARPES has much wider applicability than the traditional method using the single-particle tunneling characteristics [12]. (b) the momentum resolution of ARPES allows measurements along different directions so that the Eliashberg function $\alpha^2 F(\omega; \epsilon, \mathbf{k})$ in the whole Fermi surface for different direction can be determined. (c) Equation 3, the theoretical basis of our method, is very general and only assumes the existence of quasi-electron and its coupling with a boson field. (d) The procedure only utilizes the data of $\text{Re}\Sigma(\epsilon)$, which is easier to determine and less prone to the system imperfections than $\text{Im}\Sigma(\epsilon)$.

Our study provides new insights to EPC at the Be(10 $\bar{1}$ 0) surface: (a) the spectral structure of the Eliashberg function is significantly different from the simple fictitious models (e.g., Debye and Einstein models) previously used to interpret the data [7, 9]; (b) more than 75% (0.5 out of 0.65) of the enhanced λ is contributed by the low frequency surface modes at 20 and 40 meV that are not present in the bulk phonon spectrum. Similar behavior is also observed in Be(0001) surface [19]. This raises the question whether the low frequency surface phonon modes are responsible for the large mass enhancement factors observed in many metal surfaces [3–10]; (c) the average phonon frequency, [18]

$$\ln \omega_{\log} = \frac{2}{\lambda} \int_0^{\infty} \frac{d\omega}{\omega} \alpha^2 F(\omega) \ln \omega, \quad (9)$$

can be calculated from the extracted Eliashberg function, yielding a value 29 meV, which is substantially smaller than its bulk value (~ 60 meV) [4]. This will reduce the estimated T_c for the possible superconductivity.

In summary, we have proposed a systematic way to extract the Eliashberg function from the high-resolution ARPES data. The MEM is employed to overcome the data imperfections and numerical instability. By using this new technique, we have provided new insights to EPC at the Be(10 $\bar{1}$ 0) surface. We expect the technique would be useful in many situations, for instance, in the study of the possible role of the EPC in the

high-temperature superconductivity.

This work was supported by NSF (EWP) DMR 0105232, and the experiment was performed at the ALS of LBNL, which is operated by the DOE's Office of BES, Division of Materials Sciences and Engineering, with contract DE-AC03-76SF00098. The division also provided support for the work at SSRL. The work at Stanford was supported by NSF grant DMR-0071897. Oak Ridge National Laboratory is managed by UT-Battelle, LLC, for the U.S. Department of Energy under Contract DE-AC05-00OR22725.

-
- [1] A. Damascelli, Z. Hussain, and Z.-X. Shen, *Rev. Mod. Phys.* **75**, 473 (2003).
 - [2] T. Valla, A.V. Fedorov, P.D. Johnson, B.O. Wells, S.L. Hulbert, Q. Li, G.D. Gu, N. Koshizuka, *Science*, **285**, 2110 (1999).
 - [3] R. Matzdorf, G. Meister, A. Goldmann, *Phys. Rev. B* **54**, 14807 (1996).
 - [4] T. Balasubramanian, E. Jensen, X.L. Wu and S.L. Hulbert, *Phys. Rev. B* **57**, R6866 (1998).
 - [5] M. Hengsberger *et al.*, *Phys. Rev. Lett.* **83**, 592 (1999); M. Hengsberger, R. Fresard, D. Purdie, P. Segovia, and Y. Baer, *Phys. Rev. B* **60**, 10796 (1999).
 - [6] T. Valla, A.V. Fedorov, P.D. Johnson, S.L. Hulbert, *Phys. Rev. Lett.* **83**, 2085 (1999).
 - [7] S. LaShell, E. Jensen, and T. Balasubramanian, *Phys. Rev. B* **61**, 2371(2000).
 - [8] E. Rotenberg, J. Schaefer, S.D. Kevan, *Phys. Rev. Lett.* **84**, 2925 (2000).
 - [9] S. -J. Tang, Ismail, P. T. Sprunger, and E. W. Plummer, *Phys. Rev. B* **65**, 235428 (2002).
 - [10] C.R. Ast and H. Höchst, *Phys. Rev. B* **66**, 125103 (2002).
 - [11] D.-A. Luh, T. Miller, J. J. Paggel, T.-C. Chiang, *Phys. Rev. Lett.* **88**, 256802 (2002).
 - [12] G. Grimvall, *The Electron-Phonon Interaction in Metals*, edited by E. Wohlfarth (North-Holland, New York, 1981).
 - [13] See, for instance, J.E. Gubernatis, M. Jarrell, R.N. Silver, D.S. Sivia, *Phys. Rev. B* **44**, 6011 (1991) and references therein; M. Jarrell, J.E. Gubernatis, *Phys. Rep.* **269**, 133 (1996); M. Jarrell, preprint, http://www.physics.uc.edu/~jarrell/PAPERS/MEM_AdvPhys.pdf.
 - [14] Ph. Hofmann, E.W. Plummer, *Surf. Sci.* **377**, L330 (1997).
 - [15] A. Eiguren, B. Hellsing, F. Reinert, G. Nicolay, E.V. Chulkov, V.M. Silkin, S. Hüfner, P.M. Echenique, *Phys. Rev. Lett.* **88**, 066805 (2002).
 - [16] M. Lazzeri, S. de Gironcoli, *Surf. Sci.* **454-456**, 442 (2000).
 - [17] S. Verga, A. Knigavko, F. Marsiglio, *Phys. Rev. B* **67**, 054503 (2003).
 - [18] M.L. Kulić, *Phys. Rep.* **338**, 1 (2000).
 - [19] E.W. Plummer, unpublished.